

Size-Dependent Magnetism of Deposited Small Iron Clusters Studied by X-Ray Magnetic Circular Dichroism

J. T. Lau, A. Föhlisch, R. Nietubyè, M. Reif, and W. Wurth*

Universität Hamburg, Institut für Experimentalphysik, Luruper Chaussee 149, D-22761 Hamburg, Germany
(Received 27 September 2001; published 15 July 2002)

The size-dependent magnetic properties of small iron clusters deposited on ultrathin nickel films have been studied with circularly polarized synchrotron radiation. With the use of sum rules, orbital and spin magnetic moments have been extracted from x-ray magnetic circular dichroism spectra. The ratio of orbital to spin magnetic moments varies considerably with cluster size, reflecting the dependence of magnetic properties on cluster size and geometry. These variations can be explained in terms of enhanced orbital moments in small clusters.

DOI: 10.1103/PhysRevLett.89.057201

PACS numbers: 75.75.+a, 36.40.Cg, 61.46.+w, 87.64.Ni

Transition metal clusters are important model systems to study the evolution of magnetic and electronic properties from single atoms to bulk metals. According to Hund's rules, magnetic moments are maximized in free atoms. In bulk metals, the spin moments are weakened, leaving only iron, cobalt, and nickel as ferromagnetic elements at room temperature. In addition, the orbital magnetic moment is quenched by the crystal field. In Stern-Gerlach experiments on cluster beams [1–4], small clusters have been shown to exhibit superparamagnetic [5] behavior. Their magnetic moments are enhanced over the respective bulk values and show significant size-dependent variations. The bulk values of the magnetic moments are approached only for clusters of several hundred atoms [1–4]. Similar enhancements were also found in theoretical studies of small iron clusters [6], adatoms [7,8], nanostructures [9], and monolayers [10].

Magnetic properties of supported clusters and nanostructures are receiving considerable interest due to advances in both experimental and theoretical techniques [11]. Research in this field has been particularly stimulated by the availability of circularly polarized soft x-rays from third generation synchrotron radiation facilities, enabling investigations of magnetic properties in a polarization dependent x-ray absorption spectroscopy (XAS) experiment [12]. One of the major advantages of core level XAS over other techniques is its element specificity and its high sensitivity. With sufficiently high photon flux, even extremely diluted samples such as submonolayer coverages of size selected clusters deposited onto surfaces can be studied by XAS [13,14] and x-ray magnetic circular dichroism (XMCD). Within the theoretical framework of XMCD sum rules [15–18], the spin and orbital contributions to the magnetic moments of the cluster atoms can be separated. To probe the magnetic properties of 3d ferromagnets, XAS at the 2p edges, where electron transitions are predominantly into empty 3d states, is well suited, since the magnetic moments in this case are entirely carried by the 3d electrons.

Although thin films of larger iron nanoclusters with an average cluster size of a few hundred atoms have already been investigated by XMCD [19,20], truly size selected small transition metal clusters on surfaces have not been studied previously. Several XMCD studies, however, have been performed on ultrathin magnetic films on various substrates [21–25], characterizing their orbital and spin magnetic moments.

To study the size-dependent magnetic properties of small iron clusters, we have performed XMCD measurements on well-defined samples of *size selected* Fe_n clusters ($n = 2-9$), deposited in UHV onto out-of-plane magnetized Ni/Cu(001).

In this experiment, small Fe_n⁺ clusters are produced by Xe⁺ sputtering of a high purity (99.95%) iron target and injected into a transverse magnetic dipole field for size separation. The resulting size selected clusters are decelerated to less than 2 eV/atom, well below the iron cluster bond energies [26], and refocused onto a magnetized Ni/Cu(001) substrate. To prevent fragmentation upon deposition of the clusters, soft landing [27] is achieved by precovering the substrate with argon multilayers at ≤ 15 K. After Fe_n deposition, the argon buffer layers are desorbed by flash heating the sample to 100 K. To inhibit agglomeration and island formation, cluster coverages are chosen to be less than 0.03 monolayers (ML), i.e., three iron cluster atoms per 100 nickel surface atoms, and, except for argon desorption, the cluster sample is kept at 15–20 K throughout the experiment. It has been demonstrated by us [13,14] and other groups [27] that this experimental procedure leads to deposited clusters of well-defined size; i.e., no fragmentation or agglomeration of the clusters is observed. To minimize contamination with adsorbates, sample preparation, cluster deposition, and XMCD measurements are carried out in UHV conditions ($\leq 2 \times 10^{-10}$ mbar).

For *in situ* substrate preparation, a Cu(001) single crystal is cleaned by repeated sputter and anneal cycles. Approximately 20 layers of nickel are then grown on the

clean Cu(001) surface by evaporation from a high purity nickel foil in UHV ($p \leq 5 \times 10^{-10}$ mbar) and annealed to 400 K. Nickel and copper surface quality and cleanliness were checked with thermal desorption spectroscopy, low energy electron diffraction, and Auger electron spectroscopy. The ultrathin nickel film is magnetized perpendicular to the surface by applying a magnetic field pulse (≥ 100 mT) of a solenoid mounted in the UHV chamber. Because of their perpendicular magnetic anisotropy [28,29], these ultrathin films can be magnetized to remanence and provide the magnetic field to align the magnetic moments of the Fe_n clusters deposited onto it. For every Fe_n cluster sample that was prepared, the copper crystal was freshly cleaned, and a new nickel film was grown.

XMCD spectra were taken at the BESSY II variable polarization undulator beam line UE56/1-PGM [30] with a constant degree of 90% circular polarization. Polarization dependent x-ray absorption spectra were recorded in total and partial electron yield detection mode simultaneously. For partial electron yield detection at the iron $L_{2,3}$ edges, a retardation voltage of -200 V was applied to the detector, to enhance the Fe_n Auger electron signal over the background.

The measurement geometry is such that photons are incident along the surface normal, which is the direction of sample magnetization. Hence, depending on photon polarization, the photon helicity is oriented parallel or antiparallel to the sample magnetization. For XMCD measurements, the photon polarization was reversed while the orientation of sample magnetization remained fixed. The spectra were cross checked for systematic errors by reversing the magnetization axis of the nickel layer. XMCD scans were taken at the iron and nickel $L_{2,3}$ edges to characterize Fe_n clusters as well as the nickel underlayer.

For ultrathin films, the spin and orbit magnetic moments are strongly dependent on surface roughness and film quality [31]. To nevertheless ensure an unchanging magnetization of the Fe_n clusters, all ultrathin nickel films were grown and magnetized under the same conditions. In addition, the thickness and magnetization of the nickel underlayer was monitored for every Fe_n cluster studied. Experimental values of $m_s = 0.72\mu_B$ and $m_l = 0.13\mu_B$, which were derived for the Ni/Cu(100) underlayer from the nickel $L_{2,3}$ XMCD data using the sum rules given below, are in reasonable agreement with XMCD literature data, ranging from $(0.6-0.9)\mu_B$ for m_s and $(0.05-0.09)\mu_B$ for m_l [31-33]. The ratio of m_l to m_s equals 0.18 ± 0.1 , and is in good agreement with literature data, ranging from 0.18 to 0.22 [32].

For XMCD data analysis, the polarization dependent Fe_n XAS spectra were normalized to photon flux. To account for any x-ray absorption signal from the substrate, a background spectrum of Ni/Cu(001), clean of Fe_n clusters, was subtracted.

As an example of polarization dependent Fe_n XAS, two spectra of 0.03 ML Fe_7 on Ni/Cu(001) taken with opposite

orientation of photon helicity σ and sample magnetization M are displayed in Fig. 1. The different x-ray absorption cross sections for the two cases of parallel and antiparallel orientation of σ and M are clearly visible in these spectra. Similar to the case of Cr_n clusters deposited onto Ru(111) [14], the absorption spectra shown in Fig. 1 exhibit broad rather than atomiclike line shapes. This behavior can be ascribed to the strong electronic interaction with the substrate and should be even more pronounced for Fe_n clusters supported on ultrathin Ni/Cu(100) films.

The XMCD asymmetry of Fe_7 (i.e., the difference spectrum obtained from the two orientations of σ and M) is shown in Fig. 2. Although the coverage of Fe_7 is only 0.03 ML, the signal to noise ratio is still good, and the important XMCD features at the L_3 and L_2 edge can be distinguished with great clarity. As shown for Fe_7 , the size-dependent XMCD was measured for Fe_2 through Fe_9 . All Fe_n XMCD spectra are qualitatively similar, but differ in the size of L_3 and L_2 asymmetries. A comparison of Fe_n XMCD asymmetries with the XMCD signal of the ultrathin nickel film reveals that the coupling to the underlayer is *ferromagnetic* for all Fe_n clusters.

To obtain quantitative information on the magnetic properties of Fe_n , XMCD sum rules [15-18] for spin and orbital magnetic moments, $m_s = g_s \mu_B \cdot \langle S_z \rangle$ (where $g_s = 2$) and $m_l = \mu_B \cdot \langle L_z \rangle$, respectively, were applied. For $2p \rightarrow 3d$ excitations, these sum rules state

$$\langle L_z \rangle = 2n_h \frac{\int_{L_3+L_2} \sigma^+ - \sigma^- dE}{\int_{L_3+L_2} \sigma^+ + \sigma^0 + \sigma^- dE},$$

for the expectation value of the orbital angular momentum $\langle L_z \rangle$, and

$$\langle S_z \rangle + \frac{7}{2} \langle T_z \rangle = \frac{3}{2} n_h \times \frac{\int_{L_3} \sigma^+ - \sigma^- dE - 2 \int_{L_2} \sigma^+ - \sigma^- dE}{\int_{L_3+L_2} \sigma^+ + \sigma^0 + \sigma^- dE},$$

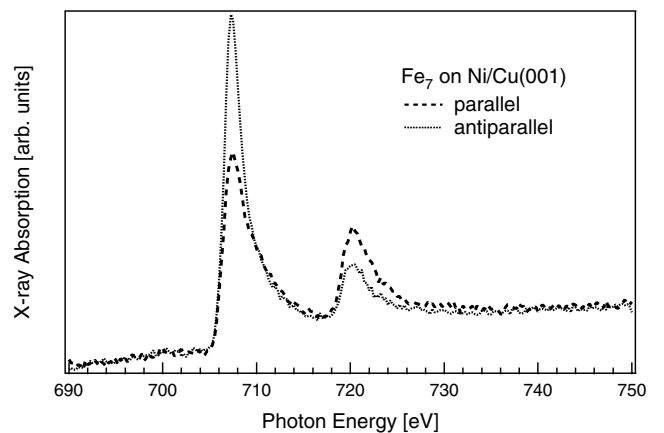


FIG. 1. Polarization dependent x-ray absorption of Fe_7 on Ni/Cu(001) at the iron L_3 and L_2 edges. Parallel (dashed line) and antiparallel (dotted line) orientation of photon helicity and magnetization.

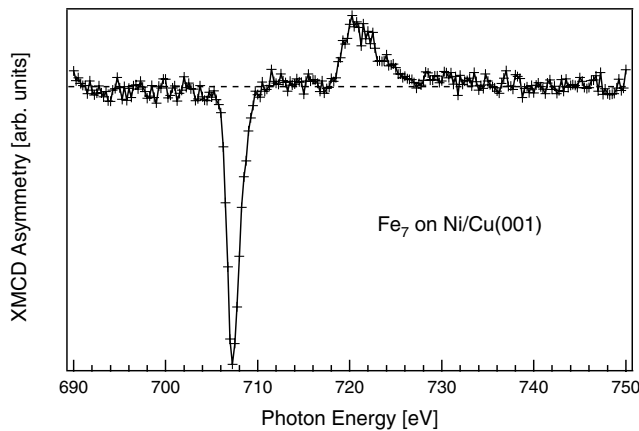


FIG. 2. XMCD asymmetry of 0.03 ML Fe₇ on Ni/Cu(001). See text.

for the expectation value of the spin angular momentum $\langle S_z \rangle$; where n_h is the number of $3d$ holes, σ^+ is a spectrum taken with parallel and σ^- with antiparallel orientation of σ and M , and σ^0 denotes a linearly polarized spectrum with photon polarization oriented parallel to the magnetization axis. Integration is over the L_3 and L_2 edges, respectively. The sum rule for the expectation value of the spin angular momentum $\langle S_z \rangle$ contains a contribution of the magnetic dipole term $\langle T_z \rangle$ which cannot be neglected for small clusters [34]. In applying these sum rules to the nickel XMCD spectra (see above), it was assumed that $\sigma^0 = 1/2(\sigma^+ + \sigma^-)$, $n_h = 1.45$ [35], and $\langle T_z \rangle = 0$ [34].

The application of XMCD sum rules to $2p \rightarrow 3d$ absorption spectra requires the total number of $3d$ holes n_h to be known in order to extract absolute values of the spin and orbital magnetic moments. Since n_h is not known for small clusters coupled to a surface, and could vary considerably as a function of cluster size, Fe_{*n*} magnetic moments will be given as moments *per 3d hole*. In addition, the ratio of orbital to spin contributions will be given as a function of cluster size. The advantage of giving these ratios as a measure of the clusters' magnetic properties is that uncertainties in cluster magnetization and photon polarization, which would contribute to an error in the absolute values, will cancel each other upon dividing m_l by m_s . The total error in m_l/m_s is estimated to be less than 20%.

The results of this sum rule analysis of Fe_{*n*} XMCD spectra are displayed in Figs. 3 and 4. Here, the ratios of m_l to m_s are plotted as a function of cluster size for Fe₂ through Fe₉. These ratios range from 0.11 to 0.27, and, in general, are larger than those observed for bulk iron [35], iron ultrathin films [21–25,36], and iron nanocluster films [19,20]. An increasing ratio of m_l to m_s is expected with decreasing dimensionality or coordination of a system [37], and this trend is visible in Fig. 3 when going from bulk iron (dash-dotted line) to small iron clusters (markers). In addition to this more general observation, there is also a nonmonotonous variation in the data displayed in Fig. 3, with the lowest ratio of m_l to m_s observed

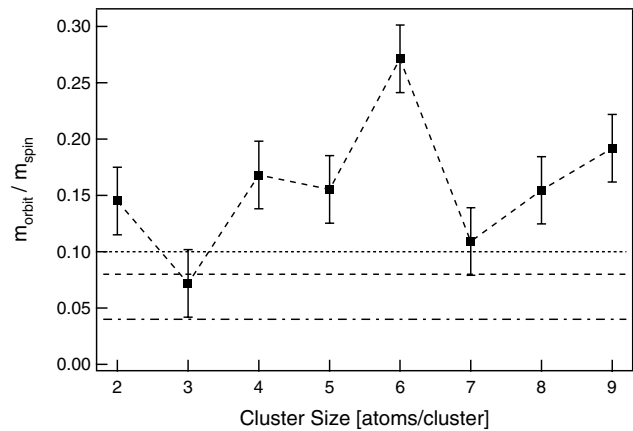


FIG. 3. Ratio of Fe_{*n*} orbital to spin magnetic moments vs cluster size as compared to bulk iron (dash-dotted line) [35], ultrathin films (dashed line) [36], and iron nanoclusters with an average cluster size of ≈ 400 (dotted line) [20].

for Fe₃, and the highest ratio for Fe₆. This variation reflects the strong dependence of electronic and magnetic properties on cluster size and geometry in the small size regime. In addition, the large changes observed in going from n to $n \pm 1$ atoms per cluster is further evidence that the sample preparation procedure yields *single sized* deposited clusters.

From calculations for small iron clusters on Ag(001), it is expected that the spin magnetic moment is enhanced over the bulk value, and is constant within 10% for small clusters supported on a substrate [9]. Furthermore, for iron atoms on Ag(100) strongly enhanced orbital moments are predicted by theory [38]. Applying these findings to Fe_{*n*} on Ni/Cu(001), we tentatively conclude that the large values of m_l to m_s plotted in Fig. 3 are due to strongly enhanced orbital magnetic moments in Fe_{*n*} on Ni/Cu(001) rather than due to reduced values of m_s . To test this, we have evaluated Fe_{*n*} magnetic moments *per 3d hole*, which are shown in Fig. 4. Indeed, the upper panel in Fig. 4 shows that, with the exception of Fe₂, the spin magnetic moments of the Fe_{*n*} clusters are fairly large (approximately $1 \mu_B/3d\text{hole}$) and vary only within 15%–20%. The lower panel in Fig. 4, on the other hand, shows that orbital moments per d -hole strongly enhanced compared to bulk and surface iron and that there is a much larger variation of these moments (by a factor of five from Fe₃ to Fe₆), which is responsible for the observed strong variation in the ratio.

The dipolar term $\langle T_z \rangle$ is a rough measure for the deviation from a spherical spin distribution [37], and therefore is very likely to be dependent on cluster geometry. Since $\langle T_z \rangle$ is included in the spin sum rule, a non-negligible contribution of $\langle T_z \rangle$ will result in a larger value of m_s [34]. In the case of Fe₂, where we observe $m_s/n_h > 1$, a large contribution of $\langle T_z \rangle$ to m_s is deduced.

It is not obvious why Fe₂ (large $\langle T_z \rangle$), Fe₃ (lowest m_l), and Fe₆ (highest m_l) should be special with respect to their magnetic properties. Although there is no direct

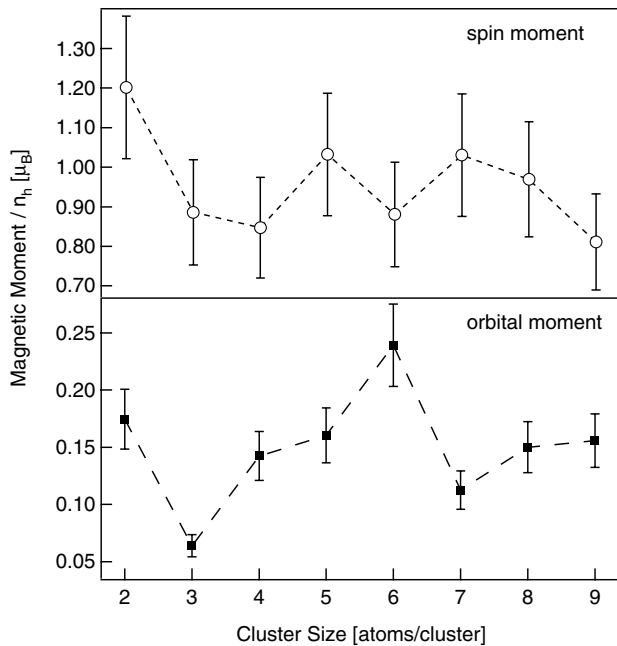


FIG. 4. Comparison of spin $(\langle S_z \rangle + \frac{7}{2} \langle T_z \rangle) / n_h$ and orbital $\langle L_z \rangle / n_h$ magnetic moments per 3d hole of Fe_n clusters on Ni/Cu(100).

information on the geometric structure of the supported clusters, we expect two-dimensional configurations where the iron atoms are located on the nickel sites (pseudomorphic arrangement). Based on this assumption one could speculate that, due to symmetry, clusters with an odd number of atoms should show different geometric arrangements and therefore different magnetic properties than even-numbered clusters, possibly leading to strongly different magnetic properties. Further experimental and theoretical investigations are needed to elucidate this finding.

In summary, we have measured orbital and spin magnetic moments as a function of cluster size for small size selected iron clusters deposited onto Ni/Cu(001). The ratios of m_l to m_s are generally larger than those observed for bulk iron, iron ultrathin films, and iron nanocluster films. There is a strong, nonmonotonous variation particularly in m_l , with strongly enhanced orbital magnetism for the clusters.

We gratefully acknowledge technical assistance from BESSY II staff members F. Senf, G. Reichardt, and M. Mast. This project was funded by BMBF through Grant No. KS1GUB/5.

*Email address: wilfried.wurth@desy.de

[1] D.M. Cox *et al.*, Phys. Rev. B **32**, 7290 (1985).

- [2] W.A. de Heer, P. Milani, and A. Châtelain, Phys. Rev. Lett. **65**, 488 (1990).
- [3] I.M.L. Billas *et al.*, Phys. Rev. Lett. **71**, 4067 (1993).
- [4] I.M.L. Billas, A. Châtelain, and W.A. de Heer, Science **265**, 1682 (1994).
- [5] C.P. Bean and J.D. Livingston, J. Appl. Phys. **30**, 120 (1959).
- [6] O. Diéguez *et al.*, Phys. Rev. B **63**, 205407 (2001).
- [7] B. Nonas *et al.*, J. Magn. Magn. Mater. **165**, 137 (1997).
- [8] M.I. Trioni, G. Palumbo, and G.P. Brivio, Surf. Sci. **433–435**, 430 (1999).
- [9] J. Izquierdo *et al.*, Phys. Rev. B **61**, 13 639 (2000).
- [10] T. Asada *et al.*, J. Phys. Condens. Matter **11**, 9347 (1999).
- [11] See, e.g., *Proceedings of the 7th International Symposium on Small Particles and Inorganic Clusters* [Surf. Rev. Lett. **3** (1996), and references therein].
- [12] G. Schütz *et al.*, Phys. Rev. Lett. **58**, 737 (1987).
- [13] J.T. Lau, A. Achleitner, and W. Wurth, Chem. Phys. Lett. **317**, 269 (2000).
- [14] J.T. Lau, A. Achleitner, and W. Wurth, Surf. Sci. **467**, 834 (2000).
- [15] B. Thole, P. Carra, and G. van der Laan, Phys. Rev. Lett. **68**, 1943 (1992).
- [16] P. Carra *et al.*, Phys. Rev. Lett. **70**, 694 (1993).
- [17] A. Ankudinov and J.J. Rehr, Phys. Rev. B **51**, 1282 (1995).
- [18] F.M.F. de Groot, J. Electron Spectrosc. Relat. Phenom. **67**, 529 (1994).
- [19] K.W. Edmonds *et al.*, J. Magn. Magn. Mater. **220**, 25 (2000).
- [20] K.W. Edmonds *et al.*, Phys. Rev. B **60**, 472 (1999).
- [21] W.L. O'Brien and B.P. Tonner, Surf. Sci. **334**, 10 (1995).
- [22] M.E. Dávila *et al.*, J. Magn. Magn. Mater. **196–197**, 120 (1999).
- [23] G.D. Waddill and J.G. Tobin, J. Appl. Phys. **73**, 6748 (1993).
- [24] J. Hunter Dunn, D. Arvanitis, and N. Mårtensson, Phys. Rev. B **54**, 11 157 (1996).
- [25] P. Ohresser *et al.*, Phys. Rev. B **62**, 5803 (2000).
- [26] L. Lian, C.-X. Su, and P.B. Armentrout, J. Chem. Phys. **97**, 4072 (1992).
- [27] H. Schaub *et al.*, Phys. Rev. Lett. **86**, 3590 (2001).
- [28] W.L. O'Brien and B.P. Tonner, Phys. Rev. B **49**, 15 370 (1994).
- [29] B. Schulz and K. Baberschke, Phys. Rev. B **50**, 13 467 (1994).
- [30] M.R. Weiss *et al.*, Nucl. Instrum. Methods Phys. Res., Sect. A **467–468**, 449 (2001).
- [31] D. Arvanitis *et al.*, J. Synchrotron Radiat. **8**, 120 (2001).
- [32] W.L. O'Brien and B.P. Tonner, Phys. Rev. B **50**, 12 672 (1994).
- [33] J. Vogel and M. Sacchi, Phys. Rev. B **49**, 3230 (1994).
- [34] R. Wu and A.J. Freeman, Phys. Rev. Lett. **73**, 1994 (1994).
- [35] P. Söderlind *et al.*, Phys. Rev. B **45**, 12 911 (1992).
- [36] C.T. Chen *et al.*, Phys. Rev. Lett. **75**, 152 (1995).
- [37] J. Stöhr, J. Magn. Magn. Mater. **200**, 470 (1999).
- [38] B. Nonas *et al.*, Phys. Rev. Lett. **86**, 2146 (2001).